SCIENTIFIC REPORTS

OPEN

High Trapped Fields in C-doped MgB$_2$ Bulk Superconductors Fabricated by Infiltration and Growth Process

A. G. Bhagurkar[1], A. Yamamoto[2], L. Wang[3], M. Xia[3], A. R. Dennis[4], J. H. Durrell [4], T. A. Aljohani[5], N. H. Babu[1] & D. A. Cardwell[4]

The grain boundaries in superconducting MgB$_2$ are known to form effective magnetic flux pinning sites and, consequently, bulk MgB$_2$ containing a fine-grain microstructure fabricated from nanoscale Mg and B precursor powders exhibits good magnetic field-trapping performance below 20 K. We report here that the trapped field of MgB$_2$ bulk superconductors fabricated by an infiltration and growth process to yield a dense, pore-free microstructure, can be enhanced significantly by carbon-doping, which increases intra-band scattering within the superconducting grains. A maximum trapped field of 4.15 T has been measured at 7.5 K at the centre of a five-sample stack of Mg(B$_{1-xi}$C$_{xi}$)$_2$ bulk superconductors processed by infiltration and growth, which not only represents a ~40% increase in trapped field observed compared to undoped bulk MgB$_2$, but also is the highest trapped field reported to date in MgB$_2$ samples processed under ambient pressure. The trapped field is observed to decay at a rate of <2%/day at 10 K, which suggests that bulk MgB$_2$ superconductors fabricated using the infiltration and growth technique can be used potentially to generate stable, high magnetic fields for a variety of engineering applications.

A bulk superconductor can act effectively as a quasi-permanent magnet when magnetized by an applied magnetic field below its superconducting transition temperature, T_c. Concentric supercurrents, induced typically throughout the bulk sample during the magnetisation process by the applied magnetic field, persist even when the external field is reduced to zero. The resulting, so-called trapped, magnetic field associated with these currents (the bulk material acts effectively as a thick, single-turn solenoid) decays extremely slowly, giving rise to a relatively stable magnetic field. Significantly, the magnitude of this trapped field is potentially much greater than that obtained typically using conventional Nd-Fe-B-based permanent magnets, which are limited generally to less than 2 T. Such compact superconducting bulk magnets are therefore excellent candidates for engineering applications where a high magnetic field is desired, such as desktop nuclear magnetic resonance (NMR), magnetic resonance imaging (MRI), motors and particle accelerators[1–3].

MgB$_2$ has been demonstrated to be a promising candidate for stable, high magnetic field applications. The key attributes from the perspective of practical applications are a combination of its high T_c, which exceeds the predictions of BCS theory due to its peculiar two band nature[4], and its tendency to form strongly linked grain boundaries, which allows the fabrication of polycrystals without the loss of inter-grain supercurrent[5,6]. As a result, a variety of methods have been developed and optimised to obtain dense, high performance MgB$_2$ bulk superconductors, such as high pressure sintering[7–10], spark plasma sintering[11] and techniques based on infiltration[12,13]. In particular, infiltration and growth (IG), impregnation or reactive liquid infiltration (RLI) processes have been developed specifically to address challenges associated with conventional sintering routes, such as porosity and poor sinterability. In this approach, B powder is packed initially to form a green body, followed by infiltration

[1]Brunel Centre for Advanced Solidification Technology, Brunel University London, Uxbridge, UB8 3PH, UK. [2]Department of Applied Physics, Tokyo University of Agriculture and Technology, 2-24-16 Nakacho, Koganei, Tokyo, 184-8588, Japan. [3]Shanghai Jiao Tong University, 800 Dong Chuan Road, Shanghai, 200240, China. [4]Department of Engineering, University of Cambridge, Trumpington Street, CB2 1PZ, Cambridge, UK. [5]National Centre for Advanced Materials, King Abdulaziz City for Science and Technology, Riyadh, 11442, Saudi Arabia. Correspondence and requests for materials should be addressed to A.G.B. (email: ashutosh.bhagurkar2@brunel.ac.uk)

Nomenclature	IG		
	B (%)	SiC (%)	B$_4$C (%)
Undoped	100	—	0
10% (B$_4$C)	90	—	10
10% (SiC)	90	10	—
20% (B$_4$C)	80	—	20
60% (B$_4$C)	40	—	60
100% (B$_4$C)	0	—	100
	MPIG		
	B (%)	MgB$_2$ (%)	B$_4$C (%)
Undoped MPIG	70	30	0
5% B$_4$C (MPIG)	65	30	5
10% B$_4$C (MPIG)	60	30	10

Table 1. Composition of the powders in the porous preforms used in IG and MPIG processes.

with liquid Mg. The vapour infiltration route, used initially for processing MgB$_2$ fibres of diameter 160 μm, was initially reported by Canfield et al.[14] and later by Dunand et al. for the synthesis of Mg-MgB$_2$ composites by infiltrating liquid Mg under pressure at 800 °C into a B preform[15]. The key advantages of this technique were demonstrated subsequently by Giunchi et al. (RLI) for the fabrication of state-of-the art bulk MgB$_2$ artefacts[12,13]. Such a relatively simple, ambient pressure process not only results in the formation of hard, dense structures but can also be applied to fabricate complex geometries that are not achieved easily using conventional sintering techniques. Bulk MgB$_2$ of relatively high density obtained by IG and RLI techniques is characterised typically by a high effective current carrying cross-sectional area, which translates directly to a higher critical current density (J_c). Although J_c in self-field as high as 10^6 A/cm^2 has been measured in bulk samples, the performance of MgB$_2$ tends to drop-off rapidly with applied magnetic field[16]. It is, therefore, essential that the in-field performance of bulk MgB$_2$ is enhanced if Nb based low temperature superconducting materials used widely in existing practical applications and which typically require expensive liquid helium (LHe) as a coolant during operation, are to be replaced.

It is well understood that the performance of MgB$_2$ can be enhanced by maximising the density of grain boundaries, which form effective pinning sites in the microstructure[17–21]. This has been achieved by employing nano-scale Mg and B precursor powders for the synthesis of MgB$_2$, which results ultimately in the formation of fine-grained MgB$_2$. Irradiation via the bombardment of neutrons, γ rays or heavy ions (Ag, Au) at sufficiently high velocities, which induces both large scale and small scale defects in the MgB$_2$ lattice, is another effective approach for improving current carrying performance of bulk MgB$_2$[22–24]. Large scale lattice defects, such as dislocations or stacking faults, act as effective pinning centres over a range of applied magnetic field and thereby improve the irreversibility field (H_{irr}) of the superconductor (i.e. an extension of its ability to generate magnetic fields for practical applications at a given temperature). Small scale lattice defects, such as point defects, on the other hand, tend to reduce the mean free path of the superconducting charge carriers, which, in turn, reduces the coherence length and results in an increased upper critical field (H_{c2})[25]. Alternatively, a superconductor can be made "dirtier", for example, by alloying to increase charge carrier scattering. Carbon doping (C-doping), in particular, has been shown to be a promising technique for enhancing J_c/H_{c2} in bulk MgB$_2$. Increased intra-band scattering (particularly in the σ band[26]), degradation of crystallinity[27–29], enhanced vortex and k pinning[30], reduced anisotropy in critical fields[31], strengthened grain boundary pinning[32] are some of the mechanisms that have led to much improved $J_c(B)$ performance in C-doped MgB$_2$ bulk superconductors. In addition, formation of defects in the microstructure such as stacking faults and nano-inclusions further contribute to pinning[33,34]. Since C in graphite allotropic form is difficult to dope into bulk MgB$_2$[35], it is often introduced in other forms that include SiC[33], C-nanotube[36], nano-diamond[37] and organic compounds[38].

In the present work, high quality Mg(B$_{1−xi}$C$_{xi}$)$_2$ (where x_i is C occupancy on boron sites in MgB$_2$ lattice) bulk superconductors were fabricated using an IG process, with B$_4$C and SiC compounds as a source of C. Changes in the lattice parameters induced by carbon substitution were studied in these samples and their effects on the superconducting properties of the bulk material have been analysed in detail in an attempt to identify the level of C addition that yield optimum critical current density. The modified IG process (MPIG) was then adopted in order to facilitate uniform liquid Mg infiltration, which is necessary to produce homogeneous bulk MgB$_2$ superconductors for practical applications. Finally, trapped field measurements were performed on the doped bulk samples and the results discussed.

Experimental Methods

Sample Preparation. Crystalline β-boron (98% pure, <40 μm) and B$_4$C (99% pure, ~2 μm) powders were mixed using a mortar and pestle to obtain $(100-x)$% B - x% B$_4$C (hereafter referred to as x% (B$_4$C) precursor compositions with x varying in weight % as 0, 10, 20, 60 and 100 (Table 1). Sixth powder mixture containing β-boron and 10 wt% SiC (~30 nm) [referred to hereafter as 10% (SiC)], was also prepared, given that SiC addition had been demonstrated previously to yield effective C-doping in bulk MgB$_2$[33]. Six precursor pellets of diameter 32 mm and thickness 6 mm, each weighing 7.5 g, were pressed uniaxially from these powder mixtures under a load of 35 MPa. The porous precursors were then subject to the IG process and reacted at 850 °C for 4 h, as described in refs[39,40].
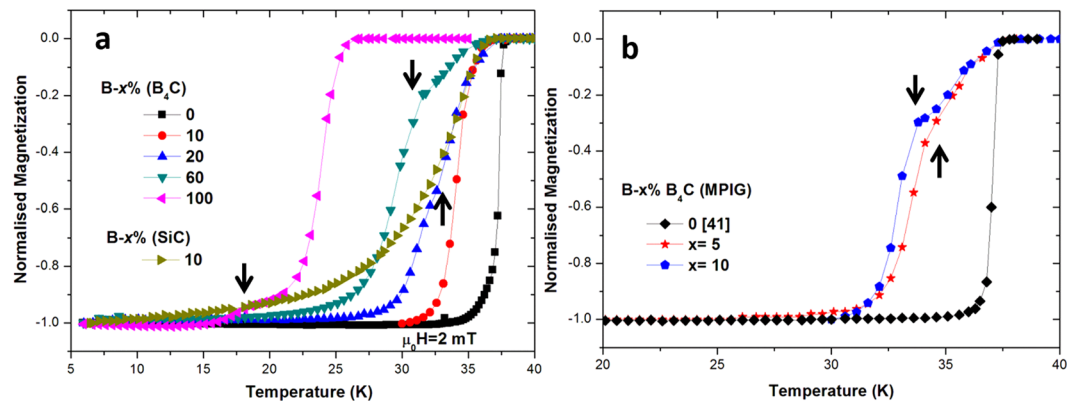
Figure 1. (**a**) Zero-field-cooled (ZFC) normalised magnetization as a function of temperature for IG samples x% (B_4C) (x: 0, 10, 20, 60 and 100) and 10% (SiC). (**b**) ZFC normalised magnetization as a function of temperature for MPIG samples. The black arrows indicate 2nd transition.

Fabrication of High Performance, Homogeneous C-doped samples.

The presence of continuous Mg channels in bulk MgB_2 processed by IG has been known[40]. These non-superconducting channels, which form during the IG process, are typically several cm in size and obstruct the flow of supercurrent in the bulk microstructure, which, in turn, limits the field trapping ability of the sample. Therefore, in order to realize the advantages offered by C-doping on a larger scale, Mg channel free MgB_2 bulk superconductors were fabricated by combining C-doping and a Modified Precursor Infiltration and Growth (MPIG) technique, as described in ref.[40]. The Addition of pre-reacted MgB_2 phase powder to the boron precursor has been shown previously to facilitate uniform in-flux of Mg, which results in the formation of homogeneous, Mg-channel free microstructure in the bulk MgB_2. As a result, appropriate mixtures of B, B_4C and MgB_2 powders were used as precursors in the MPIG process, as summarised in Table 1. 7.5 g of each precursor composition was pressed under a load of 35 MPa to obtain a pellet of diameter 32 mm and thickness 6 mm. Such C-doped bulk superconductors prepared using this method are referred to subsequently as x% B_4C (MPIG), where x is the nominal weight % of B_4C in the pellet prior to infiltration. Three bulk superconductors were fabricated by MPIG technique, one with $x = 5$, and two with $x = 10$, as described in Table 1.

Characterization.

XRD analysis ($CuK_\alpha = 1.5408$ Å) was carried out in order to identify the phases present in the sample microstructure and to enable calculation of the crystallographic lattice parameters of the fully reacted compound. The non-uniform strain/distortion in the MgB_2 lattice induced as a result of C substitution was quantified by Williamson-Hall (W-H) analysis[41]. The critical current density (J_c) of these samples was calculated from the measured magnetic moment hysteresis loops using the extended Bean model for a rectangular cross-section (Sample dimensions $\sim 3 \times 3 \times 1$ mm^3) in the presence of a magnetic field applied perpendicularly to the surface of the sample[42].

Trapped Field Measurements.

The field-cooled (FC) method was used to magnetize the C-doped MgB_2 bulk superconductors prior to the measurement of trapped magnetic field. This involved cooling down the sample, or sample arrangement, to 5 K in the presence of an external magnetic field of 5 T/6 T applied perpendicular to the top surface of the sample/samples using a Gifford–McMahon (GM) cryocooler (CRTHE05-CSFM, Iwatani Gas). The external magnetic field was then reduced to zero at a rate of 1.8 T/h to minimise any loss of trapped flux from the sample during the magnetization process (as shown in Supplementary Fig. 1). The sample was then heated slowly at a rate of 0.1 K/min and the trapped magnetic flux density measured at temperatures up to 40 K by cryogenic Hall sensors (HGCT-3020, Lake Shore).

Additional data related to this publication is available at the Brunel University London data repository (https://doi.org/10.17633/rd.brunel.5395564).

Results and Discussion

Effect on Tc.

Figure 1(a) shows the normalised magnetization as a function of temperature for samples 10% (SiC), $x = 10$%, 20%, 60%, 100% (B_4C) and an undoped sample. Both 10% (SiC) and 10% (B_4C) resulted in a reduction of T_c (defined by onset of superconducting transition) from 37.9 K (undoped) to 36.2 K, arising from σ band filling by electron doping[43]. Electron doping reduces simultaneously the number of holes at the top of the σ bands and the electronic density of states[44]. Moreover, 10% (B_4C) exhibited a relatively sharp superconducting transition, whereas 10% (SiC) showed a very broad transition, suggesting that C-doping is much less uniform in the sample containing SiC compared to that containing B_4C. This can be explained by a homogeneous distribution of C at the atomic scale in the case of B_4C. All the samples containing varying amounts of B_4C exhibited a reasonably sharp superconducting transition with T_c reducing from 37.9 K (Undoped) to 25.9 K [100% (B_4C)] as a result of C-doping in MgB_2. Moreover, the addition of B_4C with $x \geq 20$ produced two distinct transition temperatures, suggesting possible presence of two types of $Mg(B_{1-xi}C_{xi})_2$ phases. The normalised magnetization as a function of temperature for MPIG samples is shown in Fig. 1(b). The MPIG samples, 5% B_4C (MPIG) and 10% B_4C (MPIG), exhibited a second transition at 34.8 K and 33.8 K respectively, below the onset T_c (37.8 K). Such
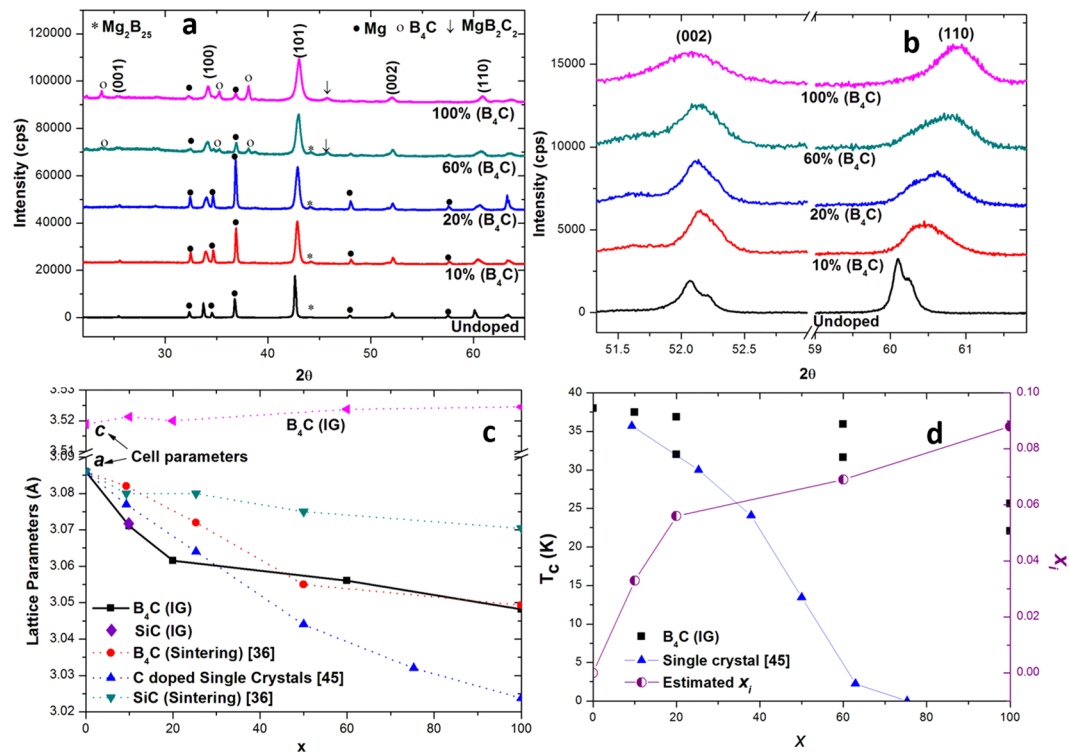
Figure 2. (**a**) XRD patterns for an undoped sample and B_4C containing samples [x% (B_4C)] revealing the presence of a majority $Mg(B_{1-xi},C_{xi})_2$ phase along with minor concentrations of Mg, B_4C and MgB_2C_2. (**b**) A significant shift observed in the (110) reflection while the (002) reflection remains almost unchanged. (**c**) Variation of the calculated lattice parameters a/c with C-doping. Data for sintered SiC/B_4C containing and single crystal samples are also shown. (**d**) Measured values of T_c in C-doped samples carbon substitution (x_i) as a function of nominal B_4C content (x).

high T_c onset of 37.8 K in MPIG samples suggests that C-doping has not taken place in the pre-reacted MgB_2. The presence of the second transition at lower temperature (34.8 K and 33.8 K), however, suggests that higher levels of C doping into MgB_2 that forms during the reaction of B with liquid Mg in the MPIG process.
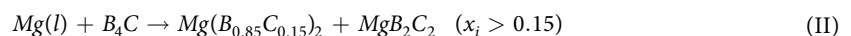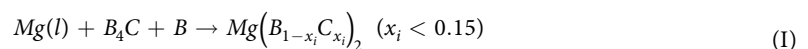
Phase analysis. Figure 2(a) compares the XRD patterns obtained for B_4C containing samples [x% (B_4C)] with an undoped sample. The undoped sample shows the presence of familiar phases: MgB_2, residual Mg and a small amount of metastable Mg_2B_{25}. On the other hand, the samples containing B_4C are composed predominantly of C-doped, superconducting $Mg(B_{1-xi},C_{xi})_2$. The equilibrium MgB_2C_2 phase and a small amount of unreacted B_4C were detected for higher nominal B_4C content of $x \geq 60$%. Figure 2(b) provides insight into nature and extent of C-doping in MgB_2. The peaks for the B_4C containing samples exhibit a component of a plane normal to the crystallographic a-b plane, and show a consistent and significant shift towards higher angles with considerable peak broadening. In addition, the peak positions corresponding to planes parallel to the basal (001) plane remain almost unchanged. This clearly suggests, and is in good agreement with previously observed studies[33,35], that C-doping induces strain in the crystallographic a-b plane only.

Figure 2(c) shows the calculated in-plane lattice parameter for MgB_2 as a function of B_4C addition [x% (B_4C)]. The data obtained are compared with those for C-doped MgB_2 single crystals and for C-doped samples produced by B_4C and SiC via a sintering route under similar reaction conditions[44]. It is apparent from the change in lattice parameter 'a' that B_4C is a more efficient dopant than SiC. Also, the C-doping level for IG samples with 10% (B_4C) and 20% (B_4C) appears to be higher than that observed in C-doped single crystals. This could be due to the fact that about 15% boron is present in the form of the intermediate boride phase, Mg_2B_{25}, which is not transformed fully into superconducting MgB_2[39]. This possibly results in an apparent increase in carbon concentration in MgB_2. Expectedly, A small change in lattice parameter 'c' was observed from 3.518 to 3.524 Å from the undoped sample to 100% (B_4C) sample. Figure 2(d) compares T_c observed in C-doped samples with nominal B_4C addition [x% (B_4C)]. The actual carbon substitution produced by B_4C addition, which is estimated by comparing the lattice parameter 'a' obtained for the present samples with that for the single crystals of $Mg(B_{1-xi}C_{xi})_2$ shown in Fig. 2(c), is also presented. The maximum carbon substitution on the B site of up to $x_i = 0.088$ was obtained for the samples containing B_4C. The effective carbon substitution (x_i) in 5% (B_4C) MPIG and 10% (B_4C) MPIG samples was estimated to be 0.022 and 0.033 respectively.

The reaction of B_4C with Mg is known to result in the formation of MgB_2 via the following chemical reactions:
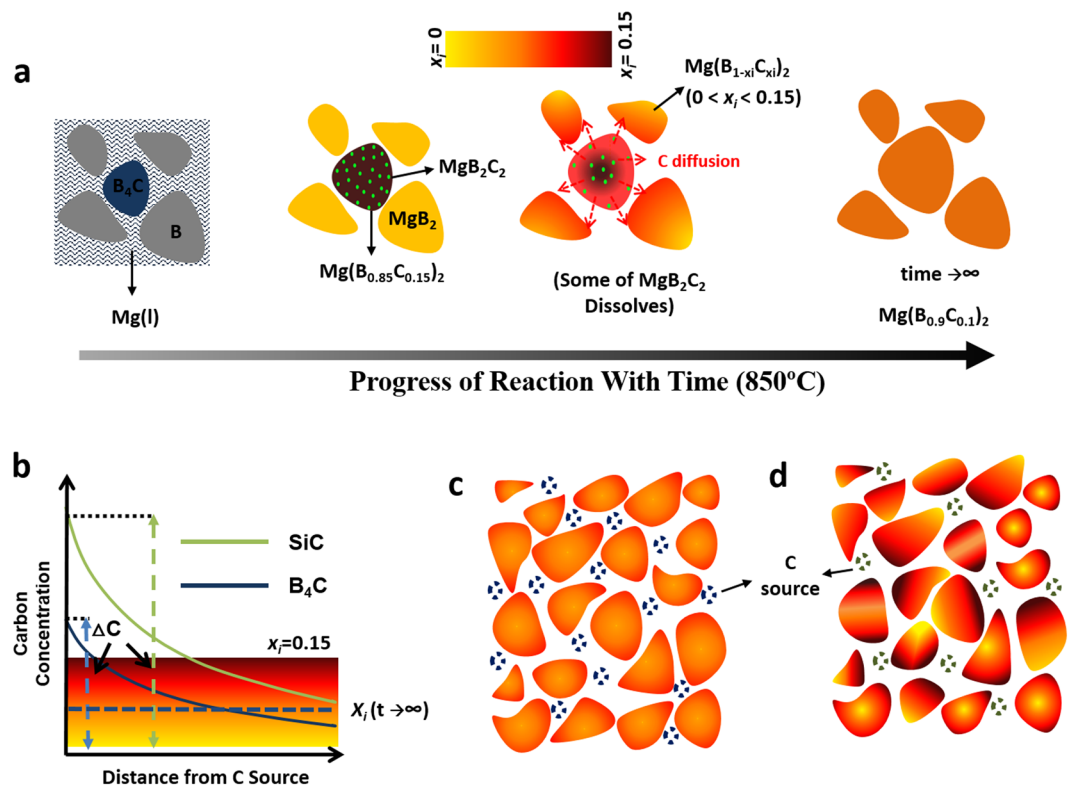
Figure 3. (**a**) Schematic illustration of C-doped MgB_2 bulk superconductor processed by infiltrating liquid Mg into Boron precursor containing 10% B_4C at 850 °C. The illustrations shown from left to right represent the various stages of reaction with time. The x_i value for 10% (B_4C) is calculated to be 0.033. (**b**) Expected carbon concentration gradients originating from two different carbon sources. The relatively large difference in ΔC is due to a large variation in C at% between the two dissimilar SiC and B_4C chemical phases. A higher degree of C variation within the $Mg(B_{1-xi}C_{xi})_2$ grain associated with (**c**) B_4C addition relative to (**d**) SiC addition is observed. Carbon sources are represented by the dashed regions. Note that the intermediate boride formation during the transformation of B to Mg_2B_{25} is not shown.

$$Mg(l) + B_4C + B \rightarrow Mg\left(B_{1-x_i}C_{x_i}\right)_2 \quad (x_i < 0.15) \tag{I}$$

$$Mg(l) + B_4C \rightarrow Mg(B_{0.85}C_{0.15})_2 + MgB_2C_2 \quad (x_i > 0.15) \tag{II}$$

Detailed analysis by Wilke *et al.*[45] suggests that an equilibrium MgB_2C_2 phase begins to appear when carbon saturation is reached, i.e. when C can no longer be accommodated in the MgB_2 lattice, which is precipitated subsequently in the form of MgB_2C_2. Analysis of C-doped MgB_2 single crystals shows that C saturation occurs at about $x_i = 0.15$[44]. In the present study, the presence of MgB_2C_2 was detected for a B_4C content of $x \geq 60$ ($x_i = 0.07$), despite the fact that the actual substitution x_i was <0.15. This suggests that carbon saturation probably occurred locally within the microstructure. Moreover, the presence of residual B_4C indicates that not all the carbon within the precursor composition doped into the MgB_2 lattice.

The mechanism of C-doping in MgB_2 from B_4C in the IG process can be understood from Figs 1 and 2, and is summarised in Fig. 3(a). Bulk Mg(l) infiltration occurs after 20–40 minutes from the beginning of the IG process[39]. This is followed by the start of the transformation of B and B_4C particles into MgB_2 and C-doped MgB_2 (Reaction II), respectively. The excess carbon in B_4C, which cannot be accommodated in the $Mg(B_{0.85}C_{0.15})_2$ lattice, precipitates in the form of MgB_2C_2. The carbon then diffuses into neighbouring undoped MgB_2 grains. Figure 3(b) shows the expected carbon concentration gradient from C-sources the B_4C and SiC, respectively, assuming that both are added separately to B to achieve the same target x_i in the $Mg(B_{1-xi}C_{xi})_2$ phase when all the C is doped in $Mg(B_{1-xi}C_{xi})_2$ for an infinite reaction time. In this case, a steeper C-concentration gradient is expected since the atomic % of C is higher in SiC (0.5) than it is in B_4C (0.2). This results conceivably in a wider spread in ΔC and a resulting broader T_c (Fig. 1). Furthermore, it is noted that the number of C-sources with SiC addition is significantly lower than those associated with B_4C addition when the B_4C and SiC particle sizes are comparable. This is because number of moles of SiC required to achieve a target x_i is fewer than the number of moles of B_4C required to achieve the same level of doping, coupled with the smaller molar volume of SiC relative to B_4C. This is likely to result in higher composition fluctuations of x_i in the SiC containing sample [Fig. 3(c)] compared to that containing B_4C [Fig. 3(d)].
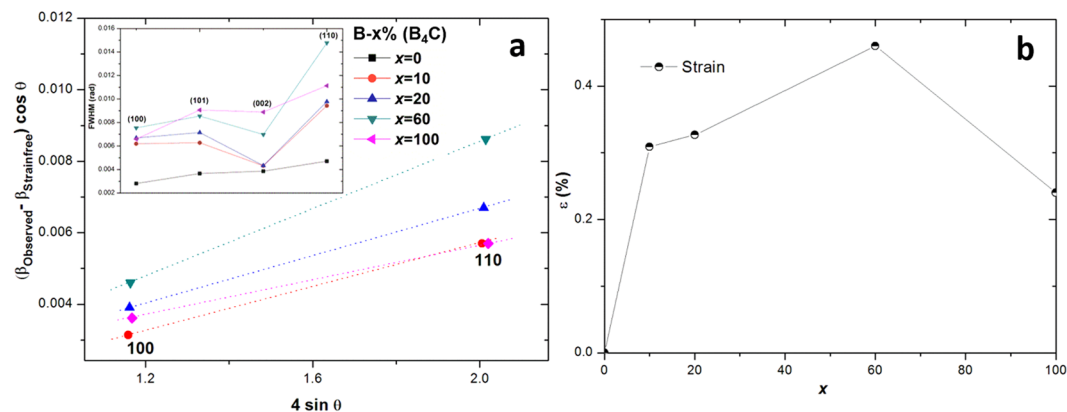
Figure 4. (**a**) A Williamson-Hall plot obtained from FWHM data for the major reflections (inset) in the XRD pattern for undoped and C-doped samples. (**b**) Non-uniform strain calculated from W-H plot as a function of nominal B_4C content.

Strain analysis.   Figure 4(a) shows the full width at half maximum (FWHM) data for various XRD reflections as a function of nominal B_4C content [x% (B_4C)]. It is apparent that C-doping has induced a large amount of lattice strain/distortion and degradation of the crystallinity in MgB_2, but mostly in the *a-b* direction, as evidenced by the increase in FWHM for the (100) and (110) reflections. In comparison, the FWHM of the (002) reflection appears rather small. The non-uniform strain/distortion in the MgB_2 lattice can be quantified by a Williamson-Hall (W-H) plot according to following equation[41]:

$$(\beta_{Observed} - \beta_{Instrumental})\cos\theta = \frac{K\,\lambda}{L} + 4\varepsilon_N \sin\theta \tag{1}$$

where $\beta_{Observed}$ and $\beta_{Instrumental}$ are the observed and instrumental broadening in radian respectively, K is the Scherrer constant determined by crystallite size (~1), λ and L are the X-ray wavelength and size of diffracting domain in Å, respectively, and ε_N is the non-uniform strain. Here, $\beta_{instrumental}$ is approximated to be the FWHM of an undoped sample, which is assumed to be strain-free. Also, since strain is present only in the *a-b* plane, only the (100) and (110) reflections are considered for the purposes of strain analysis. A W-H plot is shown for nominal B_4C content in Fig. 4(a). The C-doping was found to induce strain of up to 0.46% in the lattice, as shown in Fig. 4(b). In addition, semi-coherent precipitates (MgB_2-Mg) were detected in TEM analysis (Supplementary Fig. 2). Such a formation of semi-coherent interface further leads to localized strain in the interface region.

***Jc* and Pinning Force.**   Figure 5(a) compares J_c at 5 and 20 K as a function of external field for 10% (SiC), 10% (B_4C) and the undoped sample. It can be seen that the C-doped samples exhibit a much weaker dependence of J_c on external field, and particularly at 5 K. The sample containing B_4C, 10% (B_4C) in particular, shows a significantly enhanced self-field J_c of 600 kA/cm² (5 K) and 350 kA/cm² (20 K), which represents an increase of 50% and 36% with respect to the J_c measured in the undoped sample.

In addition, an in-field J_c (5 T, 5 K) as high as 50 kA/cm² was observed for this sample, which is nearly 10 times that observed for the undoped sample. The enhanced flux pinning, (at higher external fields, in particular) and H_{irr} is clearly a result of induced strain in the lattice, or degradation in the crystallinity of MgB_2. Such lattice imperfections enhance the intra-band scattering and reduce the electron mean free path l and coherence length ξ according to the following equation[46]:

$$\frac{1}{\xi} = \frac{1}{\xi_0} + \frac{1}{l} \tag{2}$$

A shortening of ξ allows more flux to be accommodated in the sample, which results in an increased H_{c2}. On the other hand, the sample containing SiC did not exhibit a similar improvement in J_c due to intrinsic, inhomogeneous C-doping [Fig. 1(a)]. Moreover, the reaction of SiC with Mg is known to lead to the formation of non-superconducting Mg_2Si inclusions in the bulk microstructure, which reduces the effective current carrying cross section of the sample[33,47]. Previous studies of C-doped MgB_2 bulk samples have also reported improved J_c-*B* behaviour. Nominal composition of $MgB_{1.8}(SiC)_{0.1}$ exhibited a two-fold increase in J_c (100 kA/cm² at 3 T, 20 K) compared to undoped sample. Similarly, J_c in $MgB_{1.5}(B_4C)_{0.1}$ exhibited a five-fold increase (50 kA/cm² at 5 T, 5 K) compared to J_c in undoped sample[33]. Serquis *et al.* further reported high in-field J_c of up to 50 kA/cm² (5 T, 5 K) for samples containing C-nanotube[36] and a diamond doped sample showed an improved J_c of 10 kA/cm² (20 K, 4 T), from an undoped reference J_c of 100 A/cm²[37]. A novel technique, which involved coating B with malic acid and toluene with B prior to sintering, resulted in an eight-fold increase in J_c to 40 kA/cm² (20 K, 5 T)[38].

In this study, J_c-*B* was also measured for varying B_4C content [x% (B_4C)] in order to observe any change in J_c with C-doping, as shown in Fig. 5(b). 100% (B_4C) exhibited a relatively high self-field J_c of 250 kA/cm² at 5 K, despite having a low T_c (22 K). This, together with the superconducting transitions shown [Fig. 1(a)] and the XRD
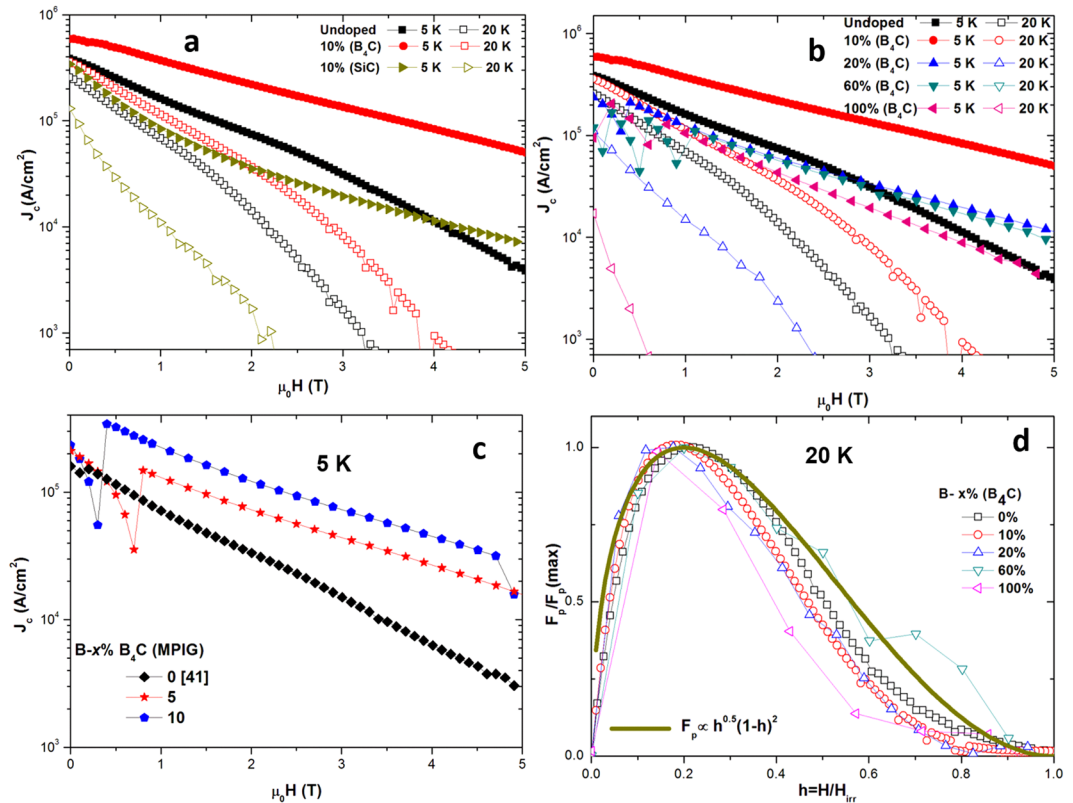
Figure 5. Measured J_c as a function of external field for samples (**a**) 10% (SiC), 10% (B_4C) (**b**) and x% (B_4C) from $x = 0$ to $x = 100$ and (**c**) J_c as a function of external fields at 5 K for MPIG samples. (**d**) Pinning force ($J_c x B$) at 20 K, as a function of reduced field ($\mu_0 H / \mu_0 H_{irr}$) for undoped and doped MgB_2 samples processed by IG.

[Fig. 2(a)] suggests that B_4C is not only highly reactive with Mg, but that the superconducting $Mg(B_{1-xi}C_{xi})_2$ phase is also well connected within the bulk microstructure. 10% (B_4C) exhibited optimum $J_c(B)$ performance, with J_c degrading gradually for higher B_4C content. This demonstrates a 'trade-off' between enhanced flux pinning and a reduction in T_c as a result of C-doping. Undoped MPIG, 5% (B_4C) MPIG and 10% (B_4C) MPIG samples, on the other hand, exhibited self-field J_c's of 200, 250 and 440 kA/cm^2, respectively at 5 K as shown in Fig. 5(c). It is apparent that the MPIG samples show reduced J_c with respect to IG samples. For instance, 10% (B_4C) and 10% B_4C (MPIG) samples showed a maximum self-field J_c of 600 and 440 kA/cm^2 respectively, at 5 K. This is because the grain boundary areas of such pre-reacted MgB_2 particles are of low J_c, due to weaker connectivity and lower H_{c2} in such areas, as suggested by the magneto-optical observations of Polyanskii et al.[48].

The variation of normalised pinning force $F_p/F_p(max)$ with reduced field ($h = H/H_{irr}$) is shown in Fig. 5(d) for undoped and C-doped samples. H_{irr} is defined as the field at which $J_c = 10^2$ A/cm^2. Dew-Hughes proposed the following equation characterising pinning forces in type II superconductors that originate from various sources[49]:

$$F_p(h) = F_p/F_{p(max)} \propto h^p (1 - h)^q \tag{3}$$

where the parameters p and q are material constants. Dew-Hughes suggested six different pinning mechanisms based on equation (3): (1) $p = 0$, $q = 2$: normal core pinning, volume pins; (2) $p = 1$, $q = 1$: Δk-pinning, volume pins (3) $p = 1/2$, $q = 2$: normal core pinning, surface pins; (4) $p = 3/2$, $q = 1$: Δk-pinning, surface pins; (5) $p = 1$, $q = 2$: normal core pinning, point pins; and (6) $p = 2$, $q = 1$: Δk-pinning, point pins.

The maximum of the normalized pinning force is expected at $h = 0.2$ for samples where surface pinning is dominant, such as that observed for undoped MgB_2 in Fig. 5(d). Such pinning is also observed in Nb-based superconductors where grain boundaries form dominant pinning sites[50]. The apparent deviation of pinning force from Dew-Hughes model results probably from anisotropy in H_{c2}, which is origin of H_{irr} in MgB_2 rather than thermally activated depinning[51]. The normalised pinning force maxima in the samples containing B_4C are shifted to lower fields at both 5 K and 20 K. For instance, 10% (B_4C) and 20% (B_4C) exhibit maxima at $h = 0.18$ and 0.15, respectively at 20 K. Such behaviour has also been reported by Matsushita et al.[52], Cheng et al. in C-doped samples[36] and Shcherbakova et al. in bulk MgB_2 containing sugar[53]. This suggests the possible presence of other, non-surface, flux pinning centres in C-doped samples, such as volume pinning. Recently, Yang et al. also observed such shift for MgB_2 containing Dy_2O_3[54]. Dy based nano-inclusions were considered to form additional pinning sites and the origin of the observed shift. In the present study, fine precipitates in the sample microstructure, such as MgB_2C_2 or unreacted B_4C could contribute towards volume pinning. Such a contribution to pinning from inclusions was reported by Dou et al. in sintered $Mg(B_{1-xi}C_{xi})_2$ containing SiC[33]. Alternatively, such a shift

in pinning force maxima towards lower field could also result from inhomogeneous C-doping, and a resultant distribution of H_{C2}, within the bulk microstructure.

High Performance homogeneous C-doped samples. Long range microstructural homogeneity and uniformity in the level and extent of carbon doping in the MgB$_2$ bulk matrix plays a critical role in determining the flux trapping potential of this material, although J_c measured in a sample of dimensions of several mm gives a good indication of this at a more local level. As a result, homogeneous, defect free C-doped MgB$_2$ bulk superconductors were fabricated by a MPIG process (Section 2.2). 5% B$_4$C (MPIG) and 10% B$_4$C (MPIG) samples were prepared in order to study the trapped field performance of bulk samples given that optimum $J_c(B)$ behaviour was obtained for 10% (B$_4$C) [Fig. 5(b)].

Trapped Field Measurements. Three sets of measurements were performed as follows - (i) 5% B$_4$C (MPIG) [Fig. 6(a)], (ii) a two-sample stack of 10% B$_4$C (MPIG) [Fig. 6(b)] and (iii) a five-sample stack [Fig. 6(c)], referred to subsequently as Stack-5. The arrangement of bulk superconductors and the location of hall probes are shown in the respective insets in Fig. 6. For the purpose of comparison, the trapped field at the centre and surface of a single, undoped bulk is shown in Fig. 6(a), whereas the trapped field at the centre and surface of a two-sample-stack of undoped bulks is shown in Fig. 6(b)[40]. A trapped magnetic flux density of 2.47 T and 2.44 T was recorded at 5 K at the centre of the top and bottom surfaces of the 5% B$_4$C (MPIG) bulk superconductor, respectively, confirming a high degree of uniformity in the sample microstructure [Fig. 6(a)]. This value of trapped field represents an increase of 16% over the one measured for the undoped MPIG sample, which decreases with temperature, reaching 0 T at 36.2 K. The two-sample stack of 10% B$_4$C (MPIG) bulk superconductors trapped 3.75 T and 2.7 T at the centre and top surface at 5 K, respectively, which represents a 25% increase over the trapped field observed in an undoped MPIG bulk of same geometrical configuration [Fig. 6(b)], which decreased relatively rapidly to reach 0 T at 34.6 K. It can be concluded, therefore, that the rate of change of trapped field with temperature ($-dB/dT$) decreases with C-doping. The observed increase in trapped field from the undoped MPIG to 10% B$_4$C (MPIG) correlates, clearly, with higher J_c at lower temperature and vice versa, and is due directly to increased C-doping in the bulk composition [Fig. 5(b)].

To date, much of the enhancement in trapped field in MgB$_2$ has been achieved by grain refinement. For instance, Fuchs *et al.* and Sugino *et al.* used nano-scale Mg and B powders produced by high energy ball milling to synthesize MgB$_2$ in an attempt to maximise grain boundary density[19,55]. These samples trapped maximum fields of 5.4 T (12 K) and 3.72 T (5 K) respectively. Similarly, Naito *et al.* observed that the addition of Ti (nominal composition Mg$_{1-xi}$Ti$_{xi}$B$_2$) resulted in the formation of a thin layer of TiB$_2$ on the MgB$_2$ crystal that pinned the grain boundaries of MgB$_2$ and inhibited grain growth[56]. Such a TiB$_2$ layer was also thought to form a vortex point pinning site. On the contrary, the increase in trapped field of Mg(B$_{1-xi}$C$_{xi}$)$_2$ bulk superconductors observed in the present study originates from atomic level intra-band scattering associated directly with C-doping. In addition, the increase has been achieved by the simple addition and mixing of B$_4$C with B powder, and without the use of expensive techniques such as high energy ball milling. This demonstrates that C-doping via B$_4$C in the IG process is an effective way of fabricating high performance MgB$_2$ bulk superconductors that can potentially generate high magnetic fields.

Finally, a five-sample stack arrangement was constructed in order to investigate the effect of thickness on the trapped field, as shown in the inset to Fig. 6(c), which is significant given the potential of bulk MgB$_2$ for application as a coaxial cylindrical superconducting magnet (which is consistent with this geometrical sample arrangement). A Hall sensor was placed on top of the 5-sample stack (H2) and another was sandwiched between the bulk superconductors (H1). A maximum trapped flux density of 4.15 T and 2.2 T was measured on H1 and H2 at 7.5 K, of which the former is the highest trapped field observed to date in MgB$_2$ bulk samples fabricated under ambient pressure. Measurement (ii) was repeated with an external field of 6 T, which was observed to have very little effect on the magnetic flux density measured at both in the centre and surface of the two-sample stack (not shown here). The trapped field of 2.32 T (H2 extrapolated to 5 K) represents a ~10% increase in the magnetic field compared to that observed in a single bulk sample. Interestingly, 4.3 T (H1 extrapolated to 5 K) represents a ~15% increase with respect to trapped field at the centre of 10% B$_4$C (MPIG) at 5 K. This suggests that such a stack arrangement could be used to generate high trapped fields in bulk MgB$_2$. Simulation studies, such as that reported in ref.[57], could be very useful to understand the distribution of magnetic flux within such a sample arrangement.

Flux Creep. Loss of flux from the superconductor occurs when the Lorentz force exceeds the flux pinning force, in which case when $J > J_c$. In addition, flux also 'leaks' at $J < J_c$ due to thermally activated flux motion. MgB$_2$, in particular, exhibits a low field decay rate compared to its high temperature superconductor counterparts at a given normalised temperature[58]. This is important from application perspective, since high temporal stability is desired in devices for Magnetic Resonance Imaging/Nuclear Magnetic Resonance, for example. Yamamoto *et al.* measured a low decay of 1.7%[59] in peak trapped field after 3 days, while Naito *et al.* noted a small decay of 2% after 40 hrs of field removal[56]. The stability of peak trapped magnetic field at the centre in the MgB$_2$ bulk samples was investigated by measuring the magnetic field relaxation at 10 K and 20 K after removal of the magnetizing field (Shown in Supplementary Figs 3 and 4). The time dependence of normalised trapped field at 10 K and 20 K for various samples is shown in Fig. 7(a,b), respectively. All the curves exhibit typical logarithmic decay (with the relevant equations given in the insets) with time ($t > 100$ s), although the variation in flux creep was observed to be non-logarithmic for $t < 100$ s. The decrease in normalised trapped field after one day at 20 K was observed to be significant greater than that observed at 10 K. For example, 5% B$_4$C (MPIG) showed a 2.3% and 3.8% reduction in trapped flux at 10 K and 20 K, respectively after 1 day. This can be explained by following equation from the Anderson-Kim model[60]:
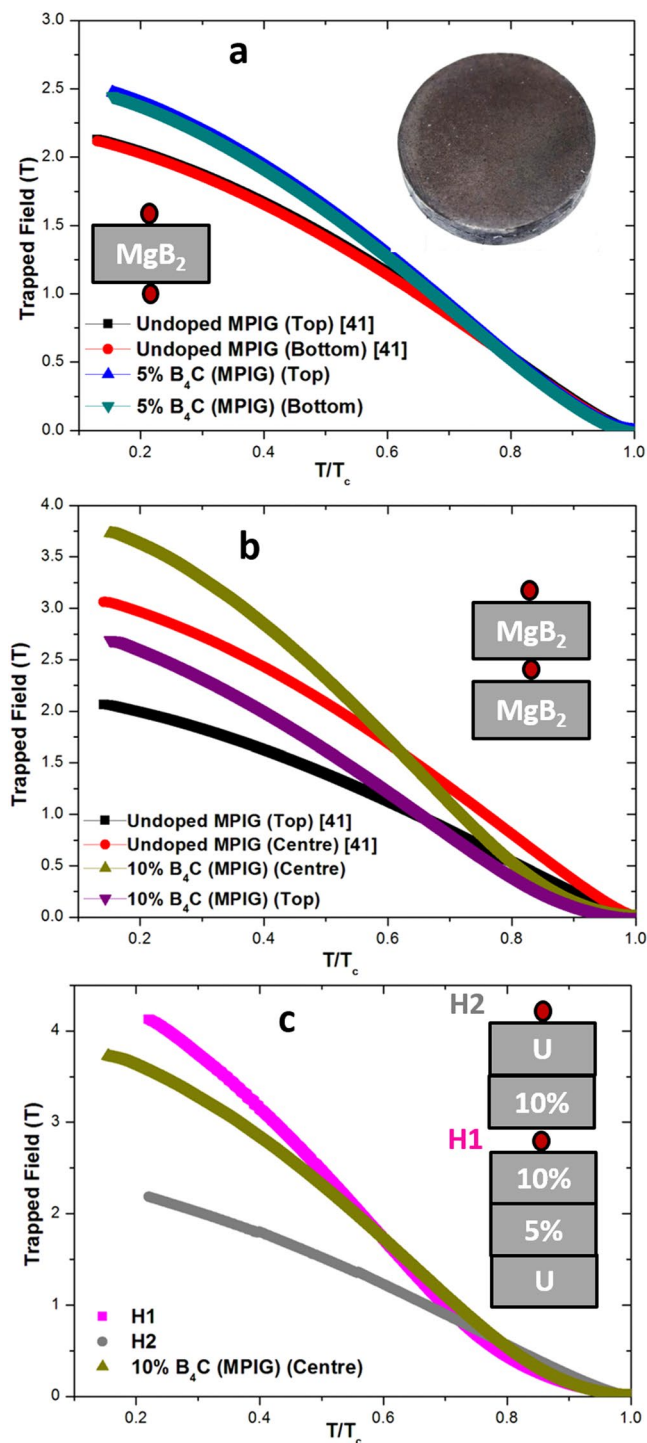
Figure 6. Maximum trapped field as a function of normalised temperature for (**a**) 5% B$_4$C (MPIG) (**b**) 10% B$_4$C (MPIG) bulk MgB$_2$ superconducting discs. Data for undoped MPIG bulk samples measured in the same configuration are also shown (**c**) Trapped field dependence with normalised temperature for a stack arrangement (Stack-5). The location of the hall probe(s) is shown in the insets and an image of representative bulk shown in (**a**). H1 was placed in the middle of gap (1.6 mm) between the two bulks.

$$\nu = \nu_0 e^{\frac{-U_0}{k_B T}} \tag{4}$$

where ν is the jump attempt frequency from one pinning site to another, U_o is the activation energy (i.e. height of the potential well) for the de-pinning of flux line and k_B is Boltzmann's constant. The trapped field is expected to
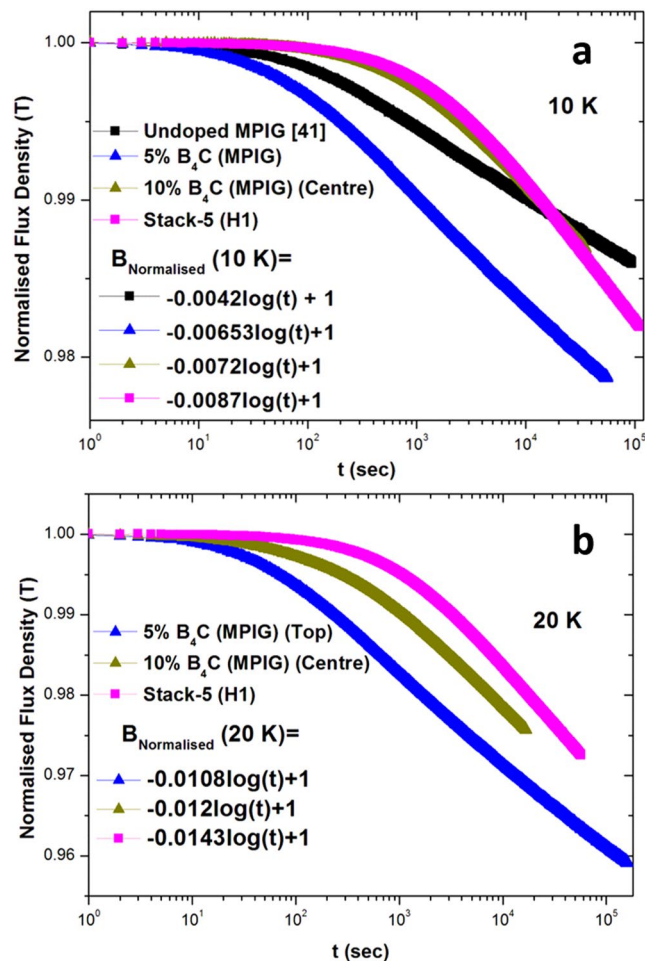
Figure 7. Time dependence of normalised field in undoped, 5% B_4C (MPIG) (top of single bulk), 10% B_4C (MPIG) (centre of stack), Stack-5 (H1) at (**a**) 10 K and (**b**) 20 K, respectively.

decay with time since the flux jump frequency increases with temperature. Interestingly, the creep rate was also found to increase with C-doping, although stronger grain boundary pinning is expected for these samples.

Conclusion

C-doped MgB_2 samples were prepared by IG technique using B_4C and SiC as sources of C. Samples fabricated using B_4C showed a more homogeneous C distribution compared to those containing SiC. This is attributed to the higher reactivity of B_4C with Mg and an atomically uniform distribution of C in the bulk microstructure. Various $Mg(B_{1-xi}C_{xi})_2$ phases in the B_4C containing samples were identified using XRD and their lattice parameters were calculated. These samples showed significant enhancement in J_c, particularly at lower temperature and higher fields. We account for this as being due to the generation of lattice strains and a loss of crystallinity in the MgB_2 phase accompanied by the effects of C-doping. Analysis of the pinning force also suggested the possibility of a contribution to enhanced J_c from point pinning. A significant increase in trapped field was observed in C-doped MgB_2 bulk superconductors. The trapped field obtained (4.15 T) in a stack of five stacked of bulk samples is the highest reported to date for MgB_2 bulk superconductors synthesized under ambient pressure conditions. Finally, we note that the finer particle size of B_4C is likely to yield more efficient and uniform C-doping, without the formation of MgB_2C_2 and leaving residual B_4C. This, together with nano-sized boron powder, would potentially yield an optimum combination of enhanced grain boundary pinning and increased H_{c2}, which could extend significantly the performance boundaries of bulk MgB_2.

References

1. Iwasa, Y., Hahn, S. Y., Tomita, M., Lee, H. & Bascunan, J. A persistent-mode" magnet comprised of YBCO annuli. *IEEE Trans. Appl. Supercond.* **15**, 2352–2355 (2005).
2. Nakamura, T., Itoh, Y., Yoshikawa, M., Oka, T. & Uzawa, J. Development of a superconducting magnet for nuclear magnetic resonance using bulk high-temperature superconducting materials Concepts *Magn. Reson., Part B* **31B**, 65–70 (2007).
3. Kii, T. *et al.* Low-temperature operation of a bulk HTSC staggered array undulator. *IEEE Trans. Appl. Supercond.* **22**, 4100904 (2012).
4. Giubileo, F. *et al.* Two-gap state density in MgB_2: a true bulk property or a proximity effect? *Physical review letters* **87**, 177008–177008 (2001).
5. Kambara, M. *et al.* High intergranular critical currents in metallic MgB_2 superconductor. *Supercond. Sci. Technol.* **14**, L5–L7 (2001).

6. Larbalestier, D. C. *et al.* Strongly linked current flow in polycrystalline forms of the superconductor MgB$_2$. *Nature* **410**, 186–189 (2001).

7. Dancer, C. E. J. *et al.* A study of the sintering behaviour of magnesium diboride. *J. Europ. Cer. Soc.* **29**, 1817–1824 (2009).

8. Takano, Y., Takeya, H., Fujii, H., Kumakura, H. & Hatano, T. Superconducting properties of MgB$_2$ bulk materials prepared by high-pressure sintering. *Appl. Phys. Lett* **78**, 2914–2916 (2001).

9. Jung, C. U. *et al.* Effect of Sintering under high pressure on the superconductivity of MgB$_2$. *Appl. Phys. Lett.* **78**, 4157–4159 (2001).

10. Liao, X. Z. *et al.* Defect structures in MgB$_2$ wires introduced by hot isostatic pressing. *Supercond. Sci. Technol.* **16**, 799–803 (2003).

11. Lee, S. Y., Yoo, S. I., Kim, Y. W., Hwang, N. M. & Kim, D. Y. Preparation of dense MgB$_2$ bulk superconductors by spark plasma sintering 2003. *J. Am. Ceram. Soc* **86**, 1800–1802 (2003).

12. Giunchi, G. High density MgB$_2$ obtained by reactive liquid Mg infiltration. *Inter. J. of Modern Phys. B* **17**, 453–460 (2003).

13. Giunchi, G., Ripamonti, G., Cavallin, T. & Bassani, E. The reactive liquid Mg infiltration process to produce large superconducting bulk MgB$_2$ manufacts. *Cryogenics* **46**, 237–242 (2006).

14. Canfield, P. C. *et al.* Superconductivity in Dense MgB$_2$ Wires. *Phys. Rev. Lett.* **86**, 2423–2426 (2001).

15. Dunand, D. C. Synthesis of superconducting Mg-MgB$_2$ composites. *Appl. Phys. Lett* **79**, 4186–4188 (2001).

16. Prikhna, T. A. *et al.* Nanostructural in homogeneities acting as pinning centers in bulk MgB$_2$ with low and enhanced grain connectivity. *Supercond. Sci. Technol.* **27**, 044013–044021 (2014).

17. Hassler, W. *et al.* Influence of the milling energy transferred to the precursor powder on the microstructure and the superconducting properties of MgB$_2$ wires *Supercond. Sci. Technol.* **26**, 025005–025011 (2013).

18. Wang, C. *et al.* Effect of high-energy ball milling time on superconducting properties of MgB$_2$ with low purity boron powder. *Supercond. Sci. Technol.* **25**, 035018–035024 (2012).

19. Sugino, S., Yamamoto, A., Shimoyama, J. & Kishio, K. Enhanced trapped field in MgB$_2$ bulk magnets by tuning grain boundary pinning through milling. *Supercond. Sci. Technol.* **28**, 055016–055022 (2015).

20. Fischer, C. *et al.* Preparation of MgB$_2$ tapes using a nanocrystalline partially reacted precursor. *Appl. Phys. Lett.* **83**, 1803–1805 (2003).

21. Perner, O. *et al.* Microstructure and impurity dependence in mechanically alloyed nanocrystalline MgB$_2$ superconductors. *Supercond. Sci. Technol.* **17**, 1148–1153 (2004).

22. Putti, M., Vaglio, R. & Rowell, J. M. Radiation effects on MgB$_2$: a review and a comparison with A15 superconductors. *Supercond. Sci. Technol.* **21**, 043001–043025 (2008).

23. Bugoslavsky, Y. *et al.* Enhancement of the high-magnetic-field critical current density of superconducting MgB$_2$ by proton irradiation. *Nature* **411**, 561–563 (2001).

24. Eisterer, M. *et al.* Neutron irradiation of MgB$_2$ bulk superconductors. *Supercond. Sci. Technol.* **15**, L9–L12 (2002).

25. Putti, M. *et al.* Neutron irradiation of Mg^{11}B$_2$: From the enhancement to the suppression of superconducting properties. *Appl. Phys. Lett.* **86**, 112503–112505 (2005).

26. Pallecchi, I. *et al.* Magnetoresistivity as a probe of disorder in the π and σ bands of MgB$_2$. *Phys. Rev. B* **72**, 184512 (2005).

27. Pogrebnyakov, A. V. *et al.* Properties of MgB$_2$ Thin Films with Carbon Doping. *Appl. Phys. Lett.* **85**, 2017–2019 (2004).

28. Braccini, V. *et al.* High-field superconductivity in alloyed MgB$_2$ thin films. *Phys. Rev. B* **71**, 012504 (2005).

29. Senkowicz, B. J. *et al.* Improved upper critical field in bulk-form magnesium diboride by mechanical alloying with carbon. *Appl. Phys. Lett.* **86**, 202502–202504 (2005).

30. Xiang, F. S. *et al.* Evidence for transformation from δT_c to δ_l pinning in MgB$_2$ by graphene oxide doping with improved low and high field J_c and pinning potential. *Appl. Phys. Lett.* **102**, 152601–152605 (2013).

31. Wisniewski, A. *et al.* Comparison of the influence of carbon substitution and neutron-induced defects on the upper critical field and flux pinning in MgB$_2$ single crystals. *Supercond. Sci. Technol.* **20**, 256–260 (2007).

32. Yamamoto, A. *et al.* Universal relationship between crystallinity and irreversibility field of MgB$_2$. *Appl. Phys. Lett.* **86**, 212502–212504 (2005).

33. Dou, S. X. *et al.* Enhancement of the critical current density and flux pinning of MgB$_2$ superconductor by nanoparticle SiC-doping *Appl. Phys. Lett.* **81**, 3419–3421 (2002).

34. Kim, J. H. *et al.* Microscopic role of carbon on MgB$_2$ wire for critical current density comparable to NbTi *NPG Asia. Materials* **4**, e3–e6 (2012).

35. Yamamoto, A. *et al.* Effects of B$_4$C-doping on critical current properties of MgB$_2$ superconductor. *Supercond. Sci. Technol.* **18**, 1323–1328 (2005).

36. Serquis, A. *et al.* Correlated enhancement of H_{c2} and J_c in carbon nanotube doped MgB$_2$ *Supercond. Sci. Technol* **20**, L12–L15 (2007).

37. Cheng, C. H., Yang, Y., Munroe, P. & Zhao, Y. Comparison between nano-diamond and carbon nanotube doping effects on critical current density and flux pinning in MgB$_2$ *Supercond. Sci. Technol.* **20**, 296–301 (2007).

38. Hossain, M. S. A. *et al.* The enhanced J_c and B_{irr} of in situ MgB$_2$ wires and tapes alloyed with C$_4$H$_6$O$_5$ (malic acid) after cold high pressure densification. *Supercond. Sci. Technol.* **22**, 095004–095011 (2009).

39. Bhagurkar, A. G. Microstructural evolution in infiltration-growth processed MgB$_2$ bulk superconductors. *J Am Ceram Soc.* **100**, 2451–2460 (2017).

40. Bhagurkar, A. G. A trapped magnetic field of 3 T in homogeneous, bulk MgB$_2$ superconductors fabricated by a modified precursor infiltration and growth process. *Supercond. Sci. Technol.* **29**, 035008–035015 (2016).

41. Williamson, G. K. & Hall, W. H. X-ray line broadening from filed aluminium and wolfram. *Acta metallurgica* **1**, 22–31 (1953).

42. Chen, D. X. & Goldfarb, R. B. Kim model for magnetization of type-II superconductors. *J. Appl. Phys.* **66**, 2489–2500 (1989).

43. Kortus, J., Dolgov, O. V., Kremer, R. K. & Golubov, A. A. Band Filling and interband scattering effects in MgB$_2$: carbon versus aluminum Doping. *Phys. Rev. Lett* **94**, 027002–027005 (2005).

44. Lee, S., Masui, T., Yamamoto, A., Uchiyama, H. & Tajima, S. Carbon substituted MgB$_2$ single crystals. *Physica C* **397**, 7–13 (2003).

45. Wilke, R. H. T., Budko, S. L., Canfield, P. C., Finnemore, D. K. & Hannahs, S. T. Synthesis of Mg(B$_{1−x}$C$_x$)$_2$ powders. *Physica C* **432**, 193–205 (2005).

46. Tinkham, M. Introduction to Superconductivity, New York, NY: McGraw-Hill (1996).

47. Wang, X. L. *et al.* Significant enhancement of critical current density and flux pinning in MgB$_2$ with nano-SiC, Si, and C-doping. *Physica C* **408**, 63–67 (2004).

48. Polyanskii, A. A. *et al.* Magneto-optical studies on polycrystalline MgB$_2$ bulks manufactured by different processes. *IEEE Trans. Appl. Supercond.* **17**, 2746–2749 (2007).

49. Dew-Hughes, D. Flux pinning mechanisms in type II superconductors. *Philos. Mag.* **30**, 293–305 (1974).

50. Dew-Hughes, D. The role of grain boundaries in determining J_c in high-field high-current superconductors *Philos. Mag* **55**, 459–479 (1987).

51. Eisterer, M., Zehetmayer, M. & Weber, H. W. Current percolation and anisotropy in polycrystalline MgB$_2$ *Phys. Rev. Lett.* **90**, 247002–247006 (2003).

52. Matsushita, T. *Flux Pinning in Superconductors* 2nd edn, Ch. 9.2, 384–386 (Springer, 2014).

53. Shcherbakova, O. V. *et al.* Sugar as an optimal carbon source for the enhanced performance of MgB2 superconductors at high magnetic fields. *Supercond. Sci. Technol.* **21**, 015005–015011 (2008).

54. Yang, Y., Sumption, M. D. & Collings, E. W. Influence of metal diboride Dy2O3 additions on microstructure and properties of MgB$_2$ fabricated at high temperature and under pressure. *Sci. Rep.* **6**, 29306–29316 (2016).

55. Fuchs, G. High trapped fields in bulk MgB$_2$ prepared by hot-pressing of ball-milled precursor powder. *Supercond. Sci. Technol.* **26**, 122002–122006 (2013).
56. Naito, T., Yoshida, T. & Fujishiro, H. Ti-doping effects on magnetic properties of dense MgB$_2$ bulk superconductors. *Supercond. Sci. Technol.* **28**, 095009–095016 (2015).
57. Zou, J. *et al*. Numerical modelling and comparison of MgB$_2$ bulks fabricated by HIP and infiltration growth. *Supercond. Sci. Technol.* **28**, 075009–075017 (2015).
58. Eley, S., Miura, M., Maiorov, B. & Civale, L. Universal lower limit on vortex creep in superconductors *Nature Materials* **16** 409–413 (2017)
59. Yamamoto, A., Ishihara, A., Tomita, M. & Kishio, K. Permanent magnet with MgB$_2$ bulk superconductor *Appl. Phys. Lett.* **105**, 032601–032604 (2014).
60. Anderson, P. W. Theory of flux creep in hard superconductors. *Phys. Rev. Lett.* **9**, 309 (1962).

Acknowledgements

Author Contributions

N.H.B., J.D. and D.C. developed this study. A.B. conducted the experimental work and wrote the manuscript. L.W. and M.X. carried out transmission electron microscopy and analysed the results. A.D. and A.Y. performed measurements on SQUID and trapped field measurements respectively. T.A., D.C, J.D., A.Y. and N.H.B. reviewed the manuscript.

Additional Information

Supplementary information accompanies this paper at https://doi.org/10.1038/s41598-018-31416-3.

Competing Interests: The authors declare no competing interests.

Publisher's note: Springer Nature remains neutral with regard to jurisdictional claims in published maps and institutional affiliations.